Chinese Physics C Vol. 50, No. 5 (2026)

Systematic study of proton radioactivity based on the double-folding potential model[*]

Hai-Tao Yang (杨海涛)[1†] Zhong-Xia Zhao (赵仲霞)[1] Xiao-Pan Li (李孝攀)[1] Yu-Hui Luo (罗玉辉)[1]
Xun Xue (薛迅)[1,3] Xiao-Jun Bao (包小军)[2‡]

[1]Department of Physics, Zhaotong University, Zhaotong 657000, China
[2]Department of Physics, Collaborative Innovation Center for Quantum Effects, and Key Laboratory of Low Dimensional Quantum Structures and Quantum Control of Ministry of Education, Hunan Normal University, Changsha 410081, China
[3]Department of Physics, East China Normal University, Shanghai 200241, China

Abstract: We study proton radioactivity in proton-rich nuclei with $53 \le Z \le 83$ within a semi-microscopic framework in which the emitted proton is described by a finite-size density distribution. Two proton-density prescriptions are considered, namely a Gaussian profile and a Fermi profile. We find that, when microscopic spectroscopic factors are combined with a double-folding potential based on finite-size proton and daughter densities, the Fermi-density prescription yields the best overall agreement with experiment, reducing the global root-mean-square (RMS) deviation of $\log_{10} T_{1/2}$ to $\sigma = 0.37$. In addition, a modified universal decay law that embeds the same spectroscopic factors yields an even smaller deviation, $\sigma = 0.28$, thereby providing a high-precision global description of proton-radioactivity half-lives. Specifically, we construct the proton–daughter interaction by folding a Skyrme-type effective nucleon–nucleon interaction with finite-size proton densities and spherical daughter densities, and we evaluate proton-emission half-lives within the Wentzel–Kramers–Brillouin (WKB) approximation for 39 known proton emitters in this region. State-dependent spectroscopic factors $S_p^{\rm QYB}$ and $S_p^{\rm ZHF}$, obtained from relativistic mean-field plus Bardeen–Cooper–Schrieffer (RMF+BCS) calculations, are employed to account for proton preformation. We then confront the calculated half-lives with experimental data and analyze the residuals by grouping them according to the minimum orbital angular momentum and whether the decay proceeds from the ground state or an isomeric state. Finally, we extend the universal decay law for proton emission (UDLP) by including an explicit spectroscopic-factor term, thereby obtaining a modified formula (MUDLP) that provides a compact global parametrization of experimental proton-radioactivity half-lives. Using the best-performing semi-microscopic prescription together with the MUDLP parametrization, we provide conditional half-life estimates for several candidate proton emitters near the proton drip line, where the input Q_p values are taken from AME2020. These results provide quantitative reference values for future experimental searches for new proton-radioactive nuclei.

Keywords: proton radioactivity, double-folding potential, spectroscopic (preformation) factor, UDLP

DOI: **CSTR:**

I. INTRODUCTION

Proton radioactivity is one of the most important decay modes of proton-rich nuclei far from the β-stability line and sets stringent limits on the production of increasingly exotic systems. It was first observed in 1970 in an isomeric state of ^{53}Co [1, 2]. With the rapid development of radioactive-ion-beam facilities, proton emission has since been identified from ground and low-lying isomeric states of parent nuclei in the mass region $A = 110–180$ [3]. This decay mode is characteristic of odd-Z nuclei located beyond the proton drip line and provides a powerful probe of nuclear structure, including shell structure, the coupling between bound and unbound states, and the spectroscopic-factor properties of exotic systems [4–6]. The emission process can be treated as quantum tunneling through a potential barrier, in close analogy to α decay. Numerous theoretical frameworks have been developed to describe proton radioactivity, such as the gen-

---

Received 10 December 2025; Accepted 26 February 2026

[*] The work is supported by the Natural Science Foundation of China (Grants No. 12175064, No.12363003, No.12365007 and No. U2167203), the Special Basic Cooperative Research Programs of Yunnan Provincial Undergraduate Universities' Association (Grant NO. 202101BA070001-144), Hunan Outstanding Youth Science Foundation (2022JJ10031).

[†] E-mail: yanghaitao205@163.com

[‡] E-mail: baoxiaojun@hunnu.edu.cn

eralized liquid-drop model [5, 6], the two-potential approach [7–9], distorted-wave Born approximation [10], the coupled-channels methods [11–13], the unified fission model [14, 15], the Coulomb-and-proximity-potential model [3], single-folding models [16–19], the Gamow-like model [20–22] and so on. In these approaches the barrier consists of Coulomb, nuclear, and centrifugal contributions; while the Coulomb and centrifugal parts are straightforward to construct, the nuclear potential can be modeled in various ways, including analytical expressions [7, 23], proximity potentials [24, 25], and folding potentials [19, 26]. The choice of nuclear potential is a key ingredient in improving the accuracy of half-life predictions. As a consequence, models based on different nuclear potentials can exhibit significantly different predictive performance. For example, even within the same theoretical framework, such as the Coulomb-and-proximity-potential model, different versions of the proximity-potential formula can lead to considerable differences in predictive power [27]. Inspired by our previous work on α decay [28], where a double-folding potential model based on a Skyrme-type effective nucleon–nucleon interaction (neglecting momentum and spin dependence) successfully reproduced the experimental half-lives, we extend this approach to investigate proton radioactivity. Since both α decay and proton emission are essentially quantum tunneling processes, applying the same microscopic framework is a natural extension. Traditionally, the interaction potential between the emitted proton and the daughter nucleus has often been calculated within a single-folding approximation, where the proton is treated as a point-like particle. In contrast, reaction and scattering studies of proton–nucleus systems commonly describe both participants by finite-size density distributions. For example, Patterson and Peterson employed a Gaussian charge distribution for the proton to unfold its charge structure from measured nuclear charge distributions, thereby providing standard parameter sets for use in impulse-approximation descriptions of hadron–nucleus reactions [29]. Spin-dependent Glauber-model calculations, such as those implemented in the SDGMPS code, likewise adopt Gaussian proton charge densities together with phenomenological or microscopic nuclear matter distributions as basic inputs to describe intermediate-energy proton–nucleus elastic scattering and to constrain rms radii [30]. Double-folding optical potentials frequently combine Woods–Saxon–type proton densities with nucleon densities from relativistic Hartree–Bogoliubov calculations [31]. Similar strategies have been used in decay models, where double-folding of an effective nucleon–nucleon interaction with Gaussian cluster densities provides a unified framework for α decay, heavy-cluster radioactivity, and, more recently, two-proton radioactivity [32]. These precedents show that representing both the target and the projectile (or emitted cluster) by finite-size densities is a natural and widely used choice in folding descriptions of proton–daughter interaction. Motivated by these developments, in the present work we represent the emitted proton by a finite-size density distribution, considering both two-parameter Fermi and Gaussian profiles when constructing the proton–daughter interaction within a double-folding potential model based on a Skyrme-type effective nucleon–nucleon interaction.

In addition, the spectroscopic factor, often referred to as the preformation factor, is a key quantity governing the accuracy of proton radioactivity half-life calculations. Microscopically, it can be regarded as the probability that a blocked proton in a given orbital of the parent nucleus is transferred to the corresponding empty orbital in the daughter nucleus [8]. At present, two major categories of methods have been developed for its determination: microscopic and phenomenological approaches. Microscopic methods are independent of the barrier-penetration model itself and are derived directly from nuclear-structure theories. They are typically based on various mean-field frameworks combined with pairing correlations, such as the relativistic mean-field theory with the Bardeen–Cooper–Schrieffer method (RMF+BCS) [6, 19, 26, 33], the relativistic continuum Hartree–Bogoliubov (RCHB) theory [34], and covariant density functional theory (CDFT) combined with BCS [35]. These approaches are capable of incorporating shell effects, deformation, and quantum mixing, thus providing a more fundamental description of the spectroscopic factor. In contrast, phenomenological methods extract the spectroscopic factor from the ratio of theoretical to experimental half-lives or propose empirical expressions that embed nuclear-structure information. Representative examples include the analytic expression proposed by Chen et al. as a function of the cube root of the daughter mass number [7], and the formula established by Zhang et al. linking the spectroscopic factor to the quadrupole deformation parameter within the deformed two-potential approach [8]. These phenomenological treatments significantly improve the reproduction of experimental data, although their results generally exhibit a certain degree of model dependence. In general, microscopic methods provide greater physical interpretability, whereas phenomenological approaches are primarily tailored to enhance predictive accuracy. In the present work, to assess the intrinsic reliability of the double-folding potential model, we employ spectroscopic factors calculated microscopically within the RMF+BCS framework by Zhang et al. [6] and Qian et al. [19] as input quantities in the evaluation of proton-radioactivity half-lives.

Analytic expressions provide a compact and complementary route to evaluate proton-emission half-lives alongside barrier-penetration models. Building on the Geiger–Nuttall law, a number of empirical or analytic formulations have been proposed for proton radioactivity; among them, the UDLP by Qi et al. [5] has been widely used as a baseline in systematic studies and as a common reference for comparison with newer formulas and models [22, 36]. A key refinement for improving global proton-radioactivity systematics is to embed explicit nuclear-structure information—especially the spectroscopic (preformation) factor—directly into the analytic description. For spherical proton emitters, Zhang and Dong demonstrated that incorporating a spectroscopic (preformation) factor, taken from microscopic RMF+BCS calculations, into the half-life formula significantly improves agreement with experiment relative to formulas that neglect preformation effects [37]. Complementary empirical systematics likewise indicate that half-life formulas which embed spectroscopic-factor and deformation dependences attain smaller RMS deviations than structure-agnostic expressions depending only on Q values and global Z, A systematics, underscoring the practical benefit of incorporating nuclear-structure information into analytic descriptions [37, 38]. Motivated by these developments, in addition to our double-folding-potential calculations we adopt the universal decay law for charged-particle emission (UDLP) as a reference analytic scaffold and extend it by an explicit spectroscopic-factor term, using values taken from published RMF+BCS calculations [6, 19], in order to improve its performance in describing proton-radioactivity half-lives.

Throughout this work, the proton-decay energy Q_p is taken from the most recent atomic-mass evaluation (AME2020). Therefore, the present calculations are intended primarily for a systematic evaluation and benchmarking of the barrier description and microscopic spectroscopic factors for known (or mass-evaluated) 1p emitters, and the reported half-lives should be interpreted as conditional on the adopted Q_p. A fully predictive description for truly unknown emitters would require theoretical Q_p values (e.g., from global mass models) or microscopic resonance approaches that determine the resonance energy and width simultaneously, which is beyond the scope of the present study.

The remainder of this paper is organized as follows. Section **2** outlines the theoretical framework. Section **3** presents numerical results and discussions. Section **4** summarizes our conclusions.

II. THEORETICAL FRAMEWORK

A. Double-folding potential model

The proton radioactivity half-lives can be calculated by

$$T_{1/2}=\frac{ln2}{\nu_0 P S_p}, \tag{1}$$

where P is the barrier penetration probability, ν_0 denotes the assault frequency of the proton inside the parent nucleus, and S_p is the spectroscopic factor of the emitted proton-daughter system. In the microscopic RMF+BCS description, the proton spectroscopic factor S_p is taken as the vacancy probability of the decaying proton orbital in the daughter nucleus. Following Refs. [6, 19], one may write $S_p=u_j^2$, where u_j^2 denotes the probability that the specific orbit associated with the emitted proton is empty in the daughter nucleus. In the present work, we directly adopt the state-dependent RMF+BCS spectroscopic factors from Zhang et al. (S_p^{ZHF}) and Qian et al. (S_p^{QYB}), and all numerical values used are explicitly listed in Table 1. The penetrability P is calculated within the Wentzel-Kramers-Brillouin (WKB) approximation and reads

$$P=\exp[-\frac{2}{\hbar}\int_{R_{in}}^{R_{out}}\sqrt{2\mu(V(r)-Q_p)}dr], \tag{2}$$

where Q_p is the release energy, and μ is the reduced mass of the system. $V(r)$ is the total interaction potential between the proton and the daughter nucleus. The classical turning points R_{in} and R_{out} are given by [39]:

$$R_{\mathrm{in}}=R_1+R_2, \tag{3}$$

and

$$R_{\mathrm{out}}=\frac{Z_1Z_2e^2}{2Q_p}+\sqrt{\left(\frac{Z_1Z_2e^2}{2Q_p}\right)^2+\frac{\hbar^2 l(l+1)}{2\mu Q_p}}, \tag{4}$$

where R_1 and R_2 are the equivalent radii of the proton and the daughter nucleus, respectively. The equivalent radii of the parent ($i=0$), emitted proton ($i=1$), and daughter nucleus ($i=2$) are taken as[39]:

$$R_i=1.28A_i^{1/3}-0.76+0.8A_i^{-1/3}\quad(\mathrm{fm}),\quad i=0,1,2. \tag{5}$$

The total interaction potential $V(r)$ consists of the Coulomb, nuclear, and centrifugal parts and is given by

$$V(r)=V_C(r)+V_N(r)+\frac{\hbar^2 l(l+1)}{2\mu r^2}, \tag{6}$$

where l presents the angular momentum, which can be obtained from the consideration of the spin-parity conservation of the decay process. The nuclear potential $V_N(r)$ between the proton and the daughter nuclei is obtained using a double-folding formalism with a Skyrme-type effective nucleon-nucleon interaction by ignoring the momentum and spin dependence, as in Refs. [40, 41]:

Table 1. Experimental proton-emission half-lives and DPM results using RMF+BCS spectroscopic factors $S_p^{\rm QYB}$ and $S_p^{\rm ZHF}$. The columns $S_p^{\rm QYB}$ and $S_p^{\rm ZHF}$ are adopted from RMF+BCS calculations in Refs. [6, 19], respectively. The calculated $\log_{10} T_{1/2}$ values are shown for two proton-density prescriptions (Gaussian and Fermi) and for the baseline choice $S_p = 1$; UDLP and MUDLP results are included for comparison.

Nucleus	Q_p (MeV)	l	$S_p^{\rm QYB}$	$S_p^{\rm ZHF}$	$\log_{10} T_{1/2}$ (s)									
					Expt	$S_p = 1$			$S_p^{\rm QYB}$			$S_p^{\rm ZHF}$		
						Gaussian	Fermi	UDLP	Gaussian	Fermi	MUDLP	Gaussian	Fermi	MUDLP
^{109}I	0.83	2	0.44	0.73	−4.03	−4.00	−4.40	−3.54	−4.39	−4.04	−3.34	−4.62	−4.27	−3.89
^{112}Cs	0.82	2	0.46	0.37	−3.31	−3.11	−3.56	−2.81	−3.53	−3.23	−2.61	−3.43	−3.13	−2.78
^{113}Cs	0.98	2	0.45	0.37	−4.77	−5.31	−5.73	−4.75	−5.72	−5.38	−4.68	−5.64	−5.30	−5.00
^{117}La	0.83	2	0.18	0.31	−1.66	−2.55	−3.02	−2.38	−2.57	−2.29	−1.77	−2.80	−2.52	−2.23
^{121}Pr	0.90	2	0.11	0.12	−1.92	−2.89	−3.39	−2.73	−2.68	−2.41	−1.94	−2.73	−2.47	−2.24
^{130}Eu	1.03	2	0.67	0.82	−3.00	−3.31	−3.84	−3.20	−3.89	−3.66	−3.30	−3.98	−3.75	−3.63
^{131}Eu	0.96	2	0.65	0.03	−1.70	−2.41	−2.94	−2.41	−2.99	−2.75	−2.44	−1.63	−1.40	−1.29
^{135}Tb	1.20	3	0.52	0.03	−3.00	−3.73	−4.53	−3.71	−4.21	−4.24	−3.84	−2.94	−2.98	−2.82
^{140}Ho	1.10	3	0.75	0.95	−2.22	−2.04	−2.85	−2.27	−2.67	−2.73	−2.47	−2.78	−2.83	−2.72
^{141}Ho	1.19	3	0.80	0.01	−2.39	−3.09	−3.89	−3.19	−3.75	−3.79	−3.50	−1.75	−1.79	−1.69
^{141}Ho$^{\rm m}$	1.26	0	0.72	0.05	−5.14	−5.71	−5.90	−5.29	−6.32	−5.76	−5.56	−5.15	−4.58	−4.76
^{145}Tm	1.75	5	0.62	0.58	−5.50	−4.77	−5.95	−4.70	−5.32	−5.74	−5.24	−5.29	−5.72	−5.42
^{146}Tm	0.90	0	0.75	0.96	−0.81	−0.40	−0.69	−0.66	−1.04	−0.56	−0.62	−1.15	−0.67	−0.81
^{146}Tm$^{\rm m}$	1.21	5	0.75	0.96	−1.14	−0.26	−1.41	−0.79	−0.90	−1.29	−1.12	−1.01	−1.40	−1.20
^{147}Tm	1.07	5	0.72	0.58	0.59	1.44	0.29	0.69	0.82	0.43	0.49	0.92	0.52	0.71
^{147}Tm$^{\rm m}$	1.13	2	0.71	0.95	−3.44	−2.72	−3.28	−2.84	−3.33	−3.13	−3.02	−3.46	−3.26	−3.34
^{150}Lu	1.29	5	0.52	0.50	−1.35	−0.49	−1.64	−1.04	−0.96	−1.35	−1.25	−0.95	−1.33	−1.21
^{150}Lu$^{\rm m}$	1.31	2	0.74	0.86	−4.40	−4.01	−4.58	−4.02	−4.63	−4.45	−4.34	−4.70	−4.52	−4.65
^{151}Lu	1.26	5	0.52	0.49	−0.90	−0.19	−1.35	−0.78	−0.66	−1.07	−0.97	−0.64	−1.04	−0.90
^{151}Lu$^{\rm m}$	1.32	2	0.75	0.86	−4.80	−4.12	−4.68	−4.12	−4.75	−4.56	−4.45	−4.81	−4.62	−4.77
^{155}Ta	1.47	5	0.38	0.42	−2.50	−1.74	−2.92	−2.18	−2.08	−2.50	−2.36	−2.12	−2.55	−2.44
^{156}Ta	1.04	2	0.68	0.76	−0.83	−0.20	−0.82	−0.68	−0.79	−0.65	−0.73	−0.84	−0.70	−0.81
^{156}Ta$^{\rm m}$	1.13	5	0.41	0.49	0.93	1.84	0.69	0.98	1.48	1.08	1.01	1.39	0.99	1.08
^{157}Ta	0.95	0	0.91	0.80	−0.53	0.27	−0.06	−0.13	−0.44	−0.02	−0.20	−0.39	0.04	−0.16
^{159}Re	1.82	5	0.23	0.31	−4.68	−4.00	−5.19	−4.15	−4.12	−4.55	−4.29	−4.25	−4.68	−4.56
^{160}Re	1.28	2	0.67	0.51	−3.16	−2.62	−3.24	−2.86	−3.20	−3.06	−3.09	−3.08	−2.94	−3.13
^{161}Re	1.22	0	0.91	0.89	−3.36	−2.84	−3.18	−2.94	−3.56	−3.14	−3.25	−3.55	−3.13	−3.42
^{161}Re$^{\rm m}$	1.34	5	0.23	0.29	−0.68	−0.09	−1.28	−0.75	−0.20	−0.63	−0.62	−0.31	−0.74	−0.67
^{164}Ir	1.84	5	0.17	0.19	−3.95	−3.78	−4.98	−4.02	−3.77	−4.20	−4.03	−3.82	−4.25	−4.20
^{165}Ir$^{\rm m}$	1.73	5	0.17	0.19	−3.43	−2.99	−4.18	−3.32	−2.98	−3.41	−3.29	−3.02	−3.45	−3.41
^{166}Ir	1.17	2	0.36	0.42	−0.82	−0.74	−1.39	−1.25	−1.06	−0.95	−1.13	−1.12	−1.00	−1.23
^{166}Ir$^{\rm m}$	1.35	5	0.19	0.19	−0.08	0.32	−0.87	−0.44	0.28	−0.15	−0.24	0.29	−0.15	−0.14
^{167}Ir	1.09	0	0.89	0.91	−1.12	−0.55	−0.92	−0.96	−1.26	−0.87	−1.14	−1.27	−0.88	−1.20
^{167}Ir$^{\rm m}$	1.26	5	0.17	0.18	0.84	1.25	0.05	0.36	1.26	0.83	0.69	1.23	0.79	0.79
^{171}Au	1.46	0	0.87	0.85	−4.65	−4.31	−4.67	−4.34	−5.01	−4.61	−4.79	−4.99	−4.59	−5.02
^{171}Au$^{\rm m}$	1.72	5	0.07	0.09	−2.59	−2.51	−3.71	−2.96	−2.08	−2.53	−2.50	−2.21	−2.65	−2.68
^{177}Tl	1.17	0	0.50	0.73	−1.17	−0.47	−0.89	−0.99	−0.92	−0.59	−0.97	−1.09	−0.75	−1.17
^{177}Tl$^{\rm m}$	1.97	5	0.02	0.02	−3.35	−3.83	−5.03	−4.16	−2.93	−3.38	−3.34	−2.93	−3.38	−3.46
^{185}Bi$^{\rm m}$	1.63	0	0.03	0.01	−4.19	−4.73	−5.09	−4.83	−4.00	−3.60	−3.94	−3.53	−3.14	−3.72

$$V_N(r) = C_0 \left\{ \frac{F_{in}-F_{ex}}{\rho_{00}} \left(\int \rho_1^2(R)\rho_2(R-r)\,dR + \int \rho_1(R)\rho_2^2(R-r)\,dR \right) + F_{ex}\int \rho_1(R)\rho_2(R-r)\,dR \right\}. \tag{7}$$

with

$$F_{in,ex} = f_{in,ex} + f'_{in,ex}\frac{N_1-Z_1}{A_1}\frac{N_2-Z_2}{A_2}, \tag{8}$$

where $Z_{1,2}$, $N_{1,2}$ and $A_{1,2}$ are the proton, neutron and mass numbers of the emitted particle and daughter nucleus, respectively. The parameters in Eqs. (7)-(8) are adopted from Ref. [41] with the values: $C_0 = 300\mathrm{MeV}\cdot\mathrm{fm}^3$, $f_{in}=0.09$, $f_{ex}=-2.59$, $f'_{in}=0.42$, $f'_{ex}=0.54$ and $\rho_{00}=0.17\mathrm{fm}^{-}3$. We note that the folding barrier (and hence the penetrability) is evaluated within a standard WKB treatment using a nonrelativistic Skyrme-type effective interaction, whereas the RMF+BCS spectroscopic factor S_p is introduced separately as an independent microscopic structure factor. $\rho_1(R)$ denotes an effective finite-size smearing profile for the emitted proton, while $\rho_2(R)$ denotes the matter density distribution of the daughter nucleus. Following Ref. [31], we adopt a two-parameter Fermi form for the proton profile and the daughter density:

$$\rho_1(R) = \frac{\rho_{00}}{1+exp((R-R_1)/a_1)}, \tag{9}$$

$$\rho_2(R) = \frac{\rho_{00}}{1+exp((|R-r|-R_2)/a_2)}, \tag{10}$$

Here $\rho_{00}=0.17\ \mathrm{fm}^{-3}$ is taken consistently with the saturation-density parameter entering the effective interaction in Eq. (7), and it is used as a fixed convention in the adopted Fermi profiles. The radii R_1 and R_2 are taken as the equivalent radii defined in Eq. (5), while the diffuseness parameters are fixed at $a_1=a_2=0.54$ fm [19]. We also tested $a_1=a_2=0.52$ fm and found that $a_1=a_2=0.54$ fm yields a smaller overall RMS deviation for the benchmark set; therefore, $a_1=a_2=0.54$ fm is adopted. However, for light spherical nuclei, a Gaussian form is also tested for the proton profile [29]:

$$\rho_1(R) = \rho_{0p}\exp\left[-(R/a_p)^2\right], \tag{11}$$

with $a_p=0.704$ fm [29], where ρ_{0p} is fixed by the unit normalization $4\pi\int_0^\infty \rho_1(R)R^2\,dR=1$.

The Coulomb potential is taken in the uniformly charged-sphere form used in the double-folding potential model of Ref. [42].

$$V_C(r) = \begin{cases} \dfrac{Z_1Z_2e^2}{r}, & r > R_c, \\ \dfrac{Z_1Z_2e^2}{2R_c}\left[3-\left(\dfrac{r}{R_c}\right)^2\right], & r \leqslant R_c. \end{cases} \tag{12}$$

where $R_c=R_1+R_2$ and Z_1 and Z_2 are the charge numbers of the proton and the daughter nucleus. The assault frequency ν_0 is evaluated within a quantum-mechanical approach as [39]:

$$\nu_0 = \frac{\omega}{2\pi} = \frac{(G+\frac{3}{2})\hbar}{1.2\pi\mu R_0^2}, \tag{13}$$

where R_0 is the effective radius of the parent nucleus and G is the principal quantum number. μ is the reduced mass of the emitted particle and daughter nuclei system. For details, see Ref. [39].

B. Empirical formulas for proton radioactivity

The present work is based on the UDLP, which was derived by Qi et al. from the microscopic mechanism of charged-particle emission; its expression is [5]:

$$\log_{10}T_{1/2} = a\chi' + b\rho' + c + d\frac{\ell(\ell+1)}{\rho'}, \tag{14}$$

where $\chi' = Z_d\sqrt{\frac{A_d}{(A_d+1)Q_p}}$, and $\rho' = \sqrt{\frac{A_dZ_d\left(A_d^{1/3}+1\right)}{A_d+1}}$. To improve the predictive performance for proton radioactivity, in analogy to Zhang et al. [37], we incorporate an explicit spectroscopic (preformation) factor into the UDLP; the resulting expression reads:

$$\log_{10}T_{1/2} = a\chi' + b\rho' + c + d\frac{\ell(\ell+1)}{\rho'} - \log S_p. \tag{15}$$

where a, b, c and d are adjustable parameters, whose values are determined by fitting experimental data of proton radioactivity.

Ⅲ. RESULTS AND DISCUSSION

In our previous work, a double-folding potential model (DPM) based on a Skyrme-type effective nucleon–nucleon interaction, in which momentum- and spin-dependent terms are neglected, was successfully applied to nuclear α decay and found to reproduce experimental half-lives with good accuracy. Motivated by the fact that proton radioactivity and α decay both originate from the same quantum-tunneling mechanism, in the present study we extend the DPM framework to investigate nuclear proton radioactivity. It is well known that, in the description of radioactive decay, the choice of the interaction potential between the emitted particle and the daughter nucleus is crucial for improving the accuracy of half-life calculations [7]. Within a double-folding framework, however, the adopted density distribution of the emitted particle also modifies the nuclear potential and thereby affects the predicted decay half-lives. Therefore, in this work we compute proton-emission half-lives for 39 proton emitters with $53 \leqslant Z \leqslant 83$ using the DPM with two different prescriptions for the proton density, namely a Gaussian profile and a two-parameter Fermi profile. The lower bound $Z = 53$ is chosen for the benchmark set of established proton emitters with measured half-lives, for which the microscopic RMF+BCS spectroscopic factors S_p tabulated in Ref. [6] are available in a consistent manner. For completeness, in the subsequent conditional predictions we also consider a few candidate nuclei with $Z \leqslant 52$ (e.g., Sb isotopes); these cases are not included in the global systematics or RMS evaluation. A small number of additional candidate nuclei (such as ^{108}I, ^{144}Tm, ^{159}Re^{m} and ^{170}Au^{m}) are not included, because in the subsequent analysis we require a uniform use of the state-dependent preformation factors tabulated by Zhang et al., and these nuclei do not have corresponding S_p values in that table (Ref. [6]). To assess the reliability of our calculations, we systematically compare the theoretical results with the available experimental data. The experimental proton-emission half-lives and the spin–parity assignments of the parent and daughter nuclei are taken from the latest evaluated nuclear-structure compilation NUBASE2020 [43], while the Q_p values are adopted from the most recent atomic-mass evaluation AME2020 [44]. Consequently, the calculated (and extrapolated) half-lives in this work should be viewed as conditional estimates given the adopted Q_p values, and any future revisions of Q_p will directly propagate into the predicted $\log T_{1/2}$.

In the present systematic calculations, the daughter nuclei are treated within the spherical approximation, i.e., spherical radii/densities are adopted to construct the interaction barrier. It is, however, well known that for axially deformed nuclei the nuclear radius and the barrier profile become orientation dependent, leading to an angle-dependent penetrability $P(\theta)$. Previous studies have shown that deformation and barrier orientation may thin the barrier for favorable directions and thus enhance the penetrability, resulting in shorter half-lives than the spherical estimate, especially for well-deformed emitters [3, 45, 46]. On the other hand, the quantitative impact of deformation on global agreement (e.g., RMS deviation) depends on the adopted deformation parameters, the treatment of orientation effects, and the consistency between the potential model and the structure input. Since the main purpose of this work is to establish a uniform baseline for global systematics, deformation degrees of freedom are not explicitly included for all nuclei at the present stage. Extending the present double-folding framework to deformed densities and/or orientation-averaged penetrabilities will be an important subject of our future work.

We first consider a baseline calculation with the spectroscopic factor fixed to unity ($S_p = 1$), thereby neglecting preformation effects. Within the DPM framework, we calculate proton radioactivity half-lives using the two choices of emitted-proton density, Gaussian and Fermi. The corresponding results are listed in columns 7 and 8 of Table 1. Overall, the half-lives obtained with both density prescriptions are in reasonable agreement with experiment. To quantify the global performance of the model, we evaluate the root-mean-square (RMS) deviation between theoretical and experimental half-lives according to

$$\sigma = \sqrt{\frac{1}{N}\sum_{i=1}^{N}\left(\log_{10} T^{\rm cal}_{1/2,i} - \log_{10} T^{\rm exp}_{1/2,i}\right)^2}. \tag{16}$$

A comparative analysis of the deviations shows that, when the emitted-proton density is modeled by a Gaussian or Fermi profile, the corresponding standard deviations are $\sigma_{\rm G} = 0.78$ and $\sigma_{\rm F} = 0.77$, respectively. Both values are substantially lower than the deviations reported for the CPPM ($\sigma_{\rm CPPM} = 1.075$), its deformed version CPPMDN ($\sigma_{\rm CPPMDN} = 1.275$), and the deformed two-potential approach ($\sigma = 1.253$), all evaluated with $S_p = 1$ [3, 8]. This indicates that, even at the baseline level, explicitly incorporating more realistic microscopic density information within the DPM framework already leads to a significantly improved description of proton-radioactivity half-lives. Nevertheless, the remaining deviations are still non-negligible. As can also be seen from Table 1, both density prescriptions tend to yield half-lives that are systematically smaller than the experimental values. This systematic underestimation mainly originates from setting the preformation (spectroscopic) factor to unity ($S_p = 1$), which overestimates the probability of proton formation in the parent nucleus and therefore leads to a systematic enhancement of the decay width.

To further improve the predictive power of the model, we explicitly include preformation factors in the subsequent calculations. Since the present DPM formulation does not by itself encode detailed nuclear-structure information such as shell effects, pairing, and deformation, we adopt state-dependent spectroscopic factors calculated within RMF theory combined with BCS pairing. Specifically, we use the microscopic spectroscopic factors of Qian et al. ($S_p^{\rm QYB}$) and Zhang et al. ($S_p^{\rm ZHF}$) as input preformation factors for the corresponding nuclei. This choice allows the model to assimilate essential structure information while preserving the systematic calculability of the DPM. On this basis, for each of the two proton-density prescriptions (Gaussian and Fermi), we recompute the DPM half-lives by introducing, in turn, the $S_p^{\rm QYB}$ and $S_p^{\rm ZHF}$ sets of preformation (spectroscopic) factors. The resulting half-lives are summarized in Table 1, and the corresponding RMS deviations are reported in Table 2.

From Table 2, one sees that for the present data set of 39 proton emitters, the RMS deviations for the Gaussian and Fermi densities are 0.78 and 0.77, respectively, when $S_p = 1$ is used as the baseline. When the $S_p^{\rm QYB}$ preformation factors are included, the RMS decreases to 0.57 (Gaussian) and 0.46 (Fermi), representing improvements of 26.9% and 40.3% relative to the baseline. When the $S_p^{\rm ZHF}$ preformation factors are used instead, the standard deviations drop to 0.44 (Gaussian) and 0.37 (Fermi), corresponding to improvements of 43.6% and 51.9% relative to their respective $S_p = 1$ baselines. These results demonstrate that the inclusion of state-dependent preformation factors, which embed nuclear-structure information, substantially enhances the DPM performance for both density prescriptions. In particular, the combination DPM(Fermi)+$S_p^{\rm ZHF}$ achieves $\sigma = 0.37$, which is smaller than the $\sigma = 0.443$ reported for the deformed two-potential approach that explicitly includes both deformation effects and spectroscopic factors [8]. This indicates that the spectroscopic factors of Zhang et al. lead to the most pronounced improvement and appear to be more compatible with the present DPM framework at the global level.

Recent years have witnessed several modern microscopic or semi-microscopic studies of proton radioactivity systematics. Xu et al. [47] proposed an improved Gamow-type description by incorporating a screened Coulomb (Hulthen-like) barrier with two adjustable parameters and reported RMS deviations of 0.274 for 31 spherical emitters and 0.367 for 13 deformed emitters in $\log_{10} T_{1/2}$. Delion and Dumitrescu [48] investigated universal proton-emission systematics within a penetrability–formation factorization scheme and found that centrifugal and quadrupole-deformation contributions to the action are generally much smaller than the Coulomb part, so that the global systematics can be described by an approximately universal trend within a factor-of-two accuracy. From a more fundamental viewpoint, Delion [49] further emphasized the factorization of the decay width into penetrability and reduced width and derived a nearly linear rule linking $\log_{10}\gamma^2$ to the fragmentation potential. Very recently, Ismail et al. [50] performed self-consistent HFB calculations with the Gogny D1S interaction to obtain deformed daughter densities and constructed folding potentials based on the M3Y-Paris interaction, achieving $\sigma \approx 0.41$ for a set of experimental proton emitters. In this context, the present DPM provides a complementary semi-microscopic route in which the barrier is generated from a double-folding potential using finite-size proton and daughter densities, while the nucleus-dependent structure effects are incorporated through microscopic RMF+BCS spectroscopic factors. The resulting global deviation $\sigma = 0.37$ for DPM(Fermi) plus $S_p^{\rm ZHF}$ indicates that an accurate barrier description combined with microscopic structure input is essential for a high-precision global reproduction of proton-emission half-lives.

To assess the performance of this preferred combination at the level of observables, Fig. 1 displays the residuals between the calculated and experimental half-lives, $\Delta \equiv \log_{10} T_{1/2}^{\rm cal} - \log_{10} T_{1/2}^{\rm exp}$. For the DPM calculations employing the Fermi proton density together with the $S_p^{\rm ZHF}$ preformation factors, the distribution is narrowly centered around zero, and the deviations for most nuclei satisfy $|\Delta| \lesssim 0.5$; the largest deviation is about $|\Delta| = 1.05$. The points marked by black arrows correspond to proton emission from isomeric states of a given nucleus. Except for $^{185}{\rm Bi}^m$, these isomeric emitters all lie within the ±0.5 band, indicating that for given Q_p, J^π (and hence the minimum orbital angular momentum l), and S_p, the present DPM framework provides a good description of isomeric decays as well. For the remaining outlier, $^{185}{\rm Bi}^m$, the positive residual (calculated half-life longer than experiment) can plausibly be attributed to the enhanced structure sensitivity near the $Z = 82$ shell closure, a possible deformation or configuration mismatch between the parent and daughter nuclei, and the particularly small S_p value tabulated for this state.

To further characterize possible structure-related trends, we perform a grouped analysis of the residuals according to the minimum orbital angular momentum l. In the present sample, the numbers of emitters with $l = 0,2,3,5$ are $N_{l=0} = 8$, $N_{l=2} = 13$, $N_{l=3} = 3$, and $N_{l=5} = 15$, respectively, and the corresponding RMS deviations under the preferred DPM(Fermi)+$S_p^{\rm ZHF}$ setting are listed in Table 3. Although the precise ordering of the RMS val-

Table 2. RMS deviations σ between calculated and experimental half-lives, and relative improvements $\Delta\sigma/\sigma_{S_p=1}$ for different models.

	$S_p = 1$			$S_p^{\rm QYB}$			$S_p^{\rm ZHF}$		
	Gaussian	Fermi	UDLP	Gaussian	Fermi	MUDLP	Gaussian	Fermi	MUDLP
σ	0.78	0.77	0.45	0.57	0.46	0.35	0.44	0.37	0.28
$\Delta\sigma/\sigma_{S_p=1}$				26.9%	40.3%	22.2%	43.6%	51.9%	37.8%

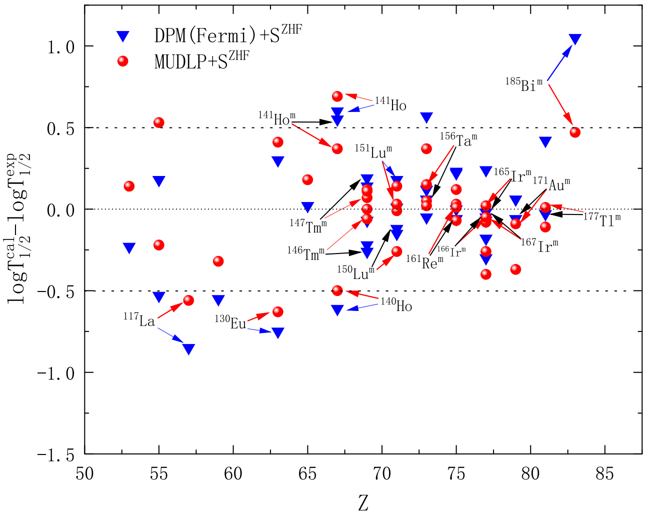

Fig. 1. (color online) Residual $\Delta = \log_{10} T^{\rm cal}_{1/2} - \log_{10} T^{\rm exp}_{1/2}$ for 39 proton emitters considered, comparing DPM(Fermi)+$S_p^{\rm ZHF}$ (triangles) and MUDLP+$S_p^{\rm ZHF}$ (circles).

Table 3. RMS deviations of Δ for different l groups.

l	5	3	2	0
N_l	15	3	13	8
RMS(Δ)	0.13	0.49	0.41	0.51

ues is affected by the limited statistics, in particular for $l = 3$ with only three emitters, the results indicate that both the centrifugal barrier and the local structure of the emitting system (e.g., deformation, configuration mixing, and pairing correlations as encoded in the RMF+BCS spectroscopic factors) play an important role in the penetrability. Consequently, they also influence the dispersion of the residuals. For the $l = 0$ and 2 subgroups, the centrifugal contribution to the barrier is relatively weak. Small variations in the decay energy Q_p and in the surface region of the double-folding potential, as well as local fluctuations in the microscopic spectroscopic factors $S_p^{\rm ZHF}$, can induce comparatively large changes in the WKB action and are more strongly reflected in $\log_{10} T_{1/2}$, naturally leading to the larger RMS deviations observed for these groups. In addition, these low-l emitters span a broad range of quadrupole deformations for both parent and daughter nuclei, and the associated structural heterogeneity is not explicitly encoded in the present DPM parametrization. By contrast, the $l = 5$ subgroup is dominated by decays assigned to well-defined high-j proton configurations, for which the adopted $S_p^{\rm ZHF}$ values are typically larger and exhibit smoother systematics in A and Z than those for the low-l emitters. The stronger centrifugal barrier also reduces the relative impact of moderate uncertainties in Q_p and in the nuclear part of the potential. These features are consistent with the smaller RMS deviation obtained for $l = 5$. Finally, for nuclei with uncertain spin–parity assignments J^π, different plausible choices of l can lead to appreciable changes in the barrier height and in the WKB action, so that the individual absolute residuals |Δ| may readily reach values of order 0.5–1.

Four ground-state proton emitters highlighted by blue arrows in Fig. 1, namely ^{117}La, ^{130}Eu, ^{140}Ho (all with $\Delta < 0$, corresponding to overestimated widths and underestimated half-lives) and ^{141}Ho ($\Delta > 0$, underestimated width), are consistent with several sensitivity mechanisms summarized in systematic studies of proton radioactivity. On the one hand, local variations of the preformation amplitude along an isotopic chain may not be fully captured by a global parametrization of S_p, so that slight overestimates or underestimates of S_p are directly mapped onto corresponding over- or underpredictions of the decay width. On the other hand, moderate nuclear deformation and configuration mismatch between the parent and daughter nuclei can modify the effective shape of the inner part of the barrier (for example, the height and thickness of the potential wall), and thus influence the penetrability through the WKB action integral. Furthermore, in the relatively low-Q_p region, small changes in the double-folding interaction near the nuclear surface (for instance, through the surface diffuseness or the effective strength of exchange-related contributions) can induce noticeable modifications of the barrier profile. Such changes are exponentially amplified in the WKB action and can lead to sizable variations in the penetrability, thereby generating relatively large residuals for a few individual nuclei. We also note that, although a Gaussian density distribution is often regarded as more suitable for describing light spherical nuclei, under the present calibration its performance for proton-radioactivity half-lives is systematically inferior to that of the two-parameter Fermi density. This likely reflects the fact that the key surface parameters used in constructing the folding potential (such as radius and diffuseness) were originally tuned under the assumption of a Fermi-type density and are therefore not optimal for the Gaussian case. To further improve the Gaussian-based results, a dedicated refit of the relevant parameters within the Gaussian-density assumption would be necessary. Motivated by the universal correlations between the decimal logarithm of half-lives and the negative decimal logarithm of penetrability reported for α decay and cluster radioactivity [45, 51], we examine the systematics between the experimental half-lives and the barrier penetrability for proton emission within the present DPM framework. We plot $\log_{10} T^{exp}_{1/2}$ as a function of $-\log_{10} P$, where P is obtained from the WKB action integral using the DPM(Fermi) potential. As shown in Fig. 2, the data exhibit a clear near-linear global trend, supporting the applicability of a universal-type behavior to proton emission within our framework. The residual scatter can be attributed to nucleus-dependent

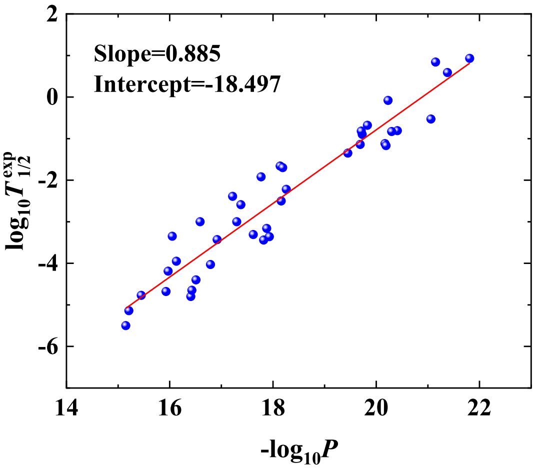

Fig. 2. (color online) $\log T^{\rm exp}_{1/2}$ versus $-\log_{10}P$ for the considered proton emitters, where P is the WKB penetrability calculated with the DPM(Fermi) potential.

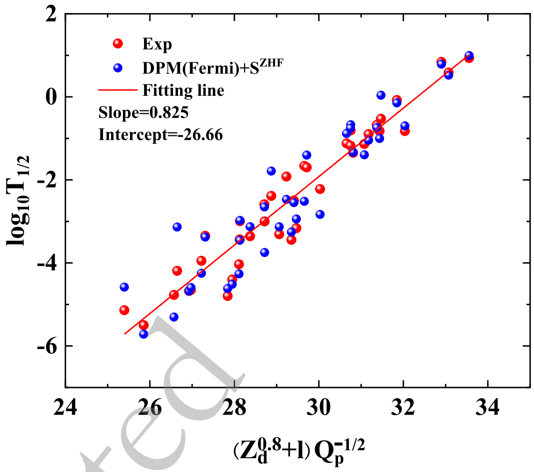

Fig. 3. (color online) Modified Geiger–Nuttall plot for proton radioactivity: $\log_{10}T_{1/2}$ as a function of $X=(Z_d^{0.8}+l)Q_p^{-1/2}$ (with Q_p in MeV). Red circles denote experimental half-lives, and blue circles denote the present DPM(Fermi)+$S_p^{\rm ZHF}$ results. The solid line is a linear fit to the experimental data.

structure effects encoded in S_p and to experimental uncertainties, consistent with the observation of Adel and Abdulghany that proton-decay systematics are generally more dispersed than those for α decay. Therefore, the observed near-linear systematics indicate that the DPM(Fermi) barrier provides a consistent global description of the penetrability governing proton emission, and can serve as a reliable baseline for systematic half-life studies. Building on the above penetrability–half-life correlation, we further examine the modified Geiger–Nuttall systematics proposed by Chen et al. [36], which explicitly accounts for the daughter charge and angular-momentum dependence, we plot $\log_{10}T^{exp}_{1/2}$ as a function of $X=(Z_d^{0.8}+l)Q_p^{-1/2}$ for all proton emitters considered in the present work. As shown in Fig. 3, the experimental half-lives exhibit an approximately linear trend in this modified GN representation. More importantly, our DPM(Fermi)+$S_p^{\rm ZHF}$ results follow the same global systematics and lie close to the experimental fitting line, indicating that the penetrabilities generated by the present DPM(Fermi) potential are consistent with the empirical modified GN behavior at the systematics level. The remaining deviations are mainly attributed to nucleus-dependent structure effects encoded in S_p and to experimental uncertainties in Q_p and spin–parity assignments. Taken together, the present results indicate that, when a two-parameter Fermi proton density is employed in combination with the preformation (spectroscopic) factors of Zhang et al., the DPM framework provides a quantitatively reliable description of nuclear proton radioactivity (with a global RMS of about 0.37 and most nuclei satisfying $|\Delta|\lesssim 0.5$), and it also provides a good description of proton emission from isomeric states. This provides a solid basis for extending the model to half-life predictions in regions closer to and beyond the current proton drip line.

In parallel with the microscopic route, we also fit an analytic UDLP to the same data set. When preformation effects are not included explicitly ($S_p=1$), the UDLP already achieves $\sigma=0.45$, which is better than the DPM baselines without preformation. When the $S_p^{\rm ZHF}$ spectroscopic factors are incorporated into UDLP, hereafter referred to as MUDLP, the dispersion is further reduced to $\sigma=0.28$, while the UDLP variant employing $S_p^{\rm QYB}$ yields $\sigma=0.35$ (see Table 2). The corresponding fitted coefficients for the original UDLP (with $S_p=1$) and for its MUDLP extension, whose parameters are obtained from a global fit including the microscopic spectroscopic factors $S_p^{\rm ZHF}$, are summarized in Table 4. The additional improvement achieved by MUDLP indicates that the analytic law can explicitly absorb slowly varying global systematic trends present in the data, such as the near-linear dependence on $A_d^{1/3}$ or surrogate fragmentation-potential variables [7] that are commonly discussed in systematics studies. In contrast, in purely barrier-penetration-based models such trends are typically only encoded implicitly through the combined effect of barrier parameters and the WKB action. We also plot in Fig. 1 the residuals obtained from MUDLP+$S_p^{\rm ZHF}$ and compare them with experiment. From Fig. 1 one can see that, when going from DPM(Fermi)+$S_p^{\rm ZHF}$ to MUDLP+$S_p^{\rm ZHF}$, the data points contract more tightly around $\Delta=\log_{10}T^{\rm cal}_{1/2}-\log_{10}T^{\rm exp}_{1/2}=0$, and most nuclei fall within the $|\Delta|\le 0.5$ band. More importantly, essentially the same set of nuclei remain the most challenging cases in both approaches (although with smaller residuals under MUDLP), which suggests that these deviations are primarily constrained by common limitations of nuclear structure or input data, rather than by deficiencies specific to either model.

Overall, on the microscopic side, the inclusion of

Table 4. Adjustable parameter values of the UDLP and MUDLP formulas.

Model	*a*	*b*	*c*	*d*
UDLP	0.38	-0.52	-16.93	2.44
MUDLP	0.43	-0.64	-18.52	2.62

state-dependent preformation factors S_p is the key lever for significantly improving the predictive accuracy of the DPM. Under the present calibration, the combination DPM(Fermi)+$S_p^{\rm ZHF}$ achieves good global performance (with $\sigma = 0.37$) and provides a physically transparent description of systematic differences between ground-state and isomeric decays. On the analytic side, the MUDLP+$S_p^{\rm ZHF}$ parametrization, which incorporates the same spectroscopic factors and smooth systematics, also achieves a small dispersion, $\sigma = 0.28$, for the same data set, while highlighting the same set of structure-limited nuclei as the DPM results. It should be emphasized that, despite the smaller statistical dispersion achieved by MUDLP+$S_p^{\rm ZHF}$ on the present data set, this approach remains an empirical interpolation formula in nature, with a more simplified treatment of barrier shapes and nuclear-structure effects. Consequently, when extrapolating beyond the region of known nuclei, its physical controllability and robustness are generally more limited than those of the DPM framework, which is based on folded potentials and an explicit WKB tunneling picture. In view of these considerations, we adopt DPM(Fermi)+$S_p^{\rm ZHF}$ as the central estimator for subsequent half-life predictions, and use MUDLP+$S_p^{\rm ZHF}$ as an independent empirical cross-check and a measure of theoretical uncertainty. The two approaches yield mutually consistent descriptions of the known proton emitters and thereby provide a robust theoretical basis for predicting proton-radioactivity half-lives of candidate nuclei beyond the present drip-line reach. On this basis, we employ both methods to predict the half-lives of several nuclei that are expected to exhibit proton radioactivity, with the aim of providing useful guidance for future experimental investigations.

For several candidate nuclei near the proton drip line whose proton radioactivity has not yet been observed, we provide half-life estimates using three prescriptions that share the same microscopic spectroscopic factors $S_p^{\rm ZHF}$ but differ in their treatment of the barrier: the DPM with Fermi- and Gaussian-type proton densities, and the analytic MUDLP formula. The adopted spins and parities of the parent and daughter nuclei are taken from NUBASE2020, while the decay energies Q_p are taken from AME2020; the spectroscopic factors are taken from Ref. [6]. For ^{104}Sb, whose spin–parity is not specified in NUBASE2020, the minimum orbital angular momentum carried by the emitted proton is taken as $l = 2$ following the configuration proposed in Ref. [6]. The corresponding values of $\log_{10} T_{1/2}$ are listed in Table 5. These estimates are conditional on the AME2020 Q_p values deduced from the available experimental mass data.

For each candidate nucleus, the three approaches yield mutually consistent results, with differences in $\log_{10} T_{1/2}$ typically of order 0.5 and not exceeding about 0.9. This spread may be regarded as a simple estimate of the present theoretical systematic uncertainty. The predicted half-lives cover a broad range of time scales, from sub-microsecond emitters such as ^{103}Sb and ^{169}Au to longer-lived cases such as ^{162,163}Re and ^{104}Sb. The largest model-to-model variation is found for ^{184}Bi, where the spread between the DPM and MUDLP predictions reaches nearly 0.9 in $\log_{10} T_{1/2}$. This enhanced sensitivity is likely associated with strong proton shell effects around the magic number $Z = 82$. In particular, proton emission from ^{184}Bi populates this closed proton shell in the daughter nucleus, and the very small spectroscopic factor $S_p^{\rm ZHF} = 0.01$ makes the calculated width especially susceptible to modest changes in the barrier parametrization. Taken together, these predictions may serve as a useful guide for future experimental searches for new proton emitters in this mass region.

Table 5. Conditional proton-emission half-life estimates for candidate proton emitters, calculated with the DPM (Fermi) +$S_p^{\rm ZHF}$ and with the MUDLP formula. The input Q_p values are taken from AME2020 (deduced from available experimental mass data), and the remaining input quantities are also listed.

Nucleus	Q_p (MeV)	J_p^π	J_d^π	l	$S_p^{\rm ZHF}$	$\log_{10} T_{1/2}^{\rm th}$ (s)		
						Gaussian	Fermi	MUDLP
^{103}Sb	0.98	5/2+#	0+	2	1.00	−6.68	−6.97	−6.56
^{104}Sb	0.51	—	5/2+#	2 [6]	1.00	1.66	1.33	1.80
^{162}Re	0.79	(2)-	7/2-#	2	0.83	4.88	4.38	4.31
^{163}Re	0.72	1/2+	0+	0	0.92	5.67	5.39	5.06
^{169}Au	1.95	1/2+#	0+	0	0.32	−7.53	−7.76	−8.30
^{184}Bi	1.56	3+#	3/2-*	1	0.01	−2.05	−2.39	−2.94

IV. SUMMARY AND CONCLUSIONS

In this work, we have extended the double–folding potential model (DPM), previously validated for α decay, to the description of proton radioactivity in nuclei with $53 \leq Z \leq 83$. The nuclear interaction between the emitted proton and the daughter nucleus is obtained by folding a Skyrme–type effective nucleon–nucleon interaction with finite–size proton densities and spherical daughter densities, and the half-lives are evaluated within the WKB approximation for 39 known proton emitters. Microscopic, state-dependent spectroscopic factors $S_p^{\rm QYB}$ and $S_p^{\rm ZHF}$ from RMF+BCS calculations are incorporated to account for the structure dependence of the proton preformation probability.

A systematic comparison with experimental half-lives shows that treating the proton as an extended object already improves the overall agreement with data compared with the Coulomb-and-proximity-potential model and with the deformed two-potential approach when the preformation factor is neglected. The inclusion of microscopic spectroscopic factors provides the main leverage for further reducing the global RMS deviation, with the combination DPM(Fermi)+$S_p^{\rm ZHF}$ emerging as the preferred setting in the present framework and achieving $\sigma = 0.37$. In parallel, we construct a modified universal decay law for proton emission (MUDLP) by introducing an explicit spectroscopic-factor term into UDLP. The resulting analytic formula closely reproduces the DPM trends and reduces the dispersion to $\sigma = 0.28$ for the same data set.

To gain qualitative insight into structure-related trends, we have analyzed the residuals grouped by the minimum orbital angular momentum l. The $l = 0$ and 2 subgroups display larger RMS deviations, which can be traced to the weaker centrifugal contribution to the barrier: small variations in Q_p, in the surface region of the double-folding potential, or in $S_p^{\rm ZHF}$ are then more strongly amplified in the WKB action and in $\log_{10} T_{1/2}$. By contrast, the $l = 5$ subgroup, dominated by well-defined high-j configurations, shows a smaller dispersion. The largest model-to-model variation is found for ^{184}Bi, where strong proton shell effects around the magic number $Z = 82$ and the very small spectroscopic factor $S_p^{\rm ZHF} = 0.01$ make the calculated width particularly sensitive to the details of the barrier.

Finally, we have used the DPM(Fermi)+$S_p^{\rm ZHF}$ and MUDLP+$S_p^{\rm ZHF}$ prescriptions to predict proton-emission half-lives for several nuclei near the proton drip line whose proton radioactivity has not yet been observed. For each candidate, the two approaches yield mutually consistent half-lives, with differences in $\log_{10} T_{1/2}$ remaining within about one order of magnitude and typically below ~ 0.9. Taken together, our results demonstrate that the DPM supplemented with microscopic spectroscopic factors provides a reliable semi-microscopic framework for describing proton radioactivity and for extrapolating towards yet-unobserved proton emitters, while the MUDLP formula offers a compact analytic complement. These predictions may serve as a useful guide for future experimental searches in the vicinity of the proton drip line. We emphasize that the present extrapolations for candidate nuclei are conditional on the adopted AME2020 Q_p values; a fully predictive description, in which both Q_p and $T_{1/2}$ are obtained self-consistently, would require coupling to nuclear-mass models or microscopic resonance approaches, which will be pursued in future work.

References

[1] K. Jackson, C. Cardinal, H. Evans, *et al.*, Phys. Lett. B **33**, 281 (1970)
[2] J. Cerny, J. Esterl, R. Gough, *et al.*, Phys. Lett. B **33**, 284 (1970)
[3] K. P. Santhosh and I. Sukumaran, Phys. Rev. C **96**, 034619 (2017)
[4] M. Karny, K. Rykaczewski, R. Grzywacz, *et al.*, Phys. Lett. B **664**, 52 (2008)
[5] C. Qi, D. S. Delion, R. J. Liotta, *et al.*, Phys. Rev. C **85**, 011303 (2012)
[6] H. F. Zhang, Y. J. Wang, J. M. Dong, *et al.*, J. Phys. G: Nucl. Part. Phys. **37**, 085107 (2010)
[7] J. L. Chen, X. H. Li, X. J. Wu, *et al.*, Eur. Phys. J. A **57**, 305 (2021)
[8] D.-M. Zhang, L. J. Qi, H. F. Gui, *et al.*, Phys. Rev. C **108**, 024318 (2023)
[9] Y. Fan, X. D. Sun, L. J. Liao, X. Liu, *et al.*, Phys. Rev. C **112**, 054311 (2025)
[10] S. Åberg, P. B. Semmes, and W. Nazarewicz, Phys. Rev. C **56**, 1762 (1997)
[11] D. Delion, R. Liotta, and R. Wyss, Physics Reports **424**, 113 (2006)
[12] C. N. Davids and H. Esbensen, Phys. Rev. C **64**, 034317 (2001)
[13] B. Barmore, A. T. Kruppa, W. Nazarewicz, *et al.*, Phys. Rev. C **62**, 054315 (2000)
[14] M. Balasubramaniam and N. Arunachalam, Phys. Rev. C **71**, 014603 (2005)
[15] J. M. DONG, H. F. ZHANG, W. ZUO, *et al.*, Chin. Phys. C **34**, 182 (2010)
[16] D. N. Basu, P. R. Chowdhury, and C. Samanta, Phys. Rev. C **72**, 051601 (2005)
[17] B. Sahu, S. K. Agarwalla, and S. K. Patra, Phys. Rev. C **84**, 054604 (2011)
[18] Y. B. QIAN, Z. Z. REN, and D. D. NI, Chin. Phys. Lett. **27**, 072301 (2010)
[19] Y. Qian and Z. Ren, Eur. Phys. J. A **52**, 68 (2016)
[20] A. Zdeb, M. Warda, C. Petrache, *et al.*, Eur. Phys. J. A **52**, 323 (2016)
[21] J. L. Chen, X. H. Li, J. H. Cheng, *et al.*, J. Phys. G: Nucl.

Part. Phys. **46**, 065107 (2019)
[22] D. M. Zhang, X. Y. Hu, L. J. Qi, *et al*., Chin. Phys. C **48**, 044102 (2024)
[23] N. Teruya, S. B. Duarte, and M. M. N. Rodrigues, Phys. Rev. C **93**, 024606 (2016)
[24] C. Guo and G. Zhang, Eur. Phys. J. A **50**, 187 (2014)
[25] D. M. Zhang, L. J. Qi, D. X. Zhu, *et al*., Nucl. Sci. Tech **34**, 55 (2023)
[26] A. Soylu, F. Koyuncu, G. Gangopadhyay, *et al*., Chin. Phys. C **45**, 044108 (2021)
[27] J. G. Deng, X. H. Li, J. L. Chen, *et al*., Eur. Phys. J. A **55**, 58 (2019)
[28] H. Yang, X. Li, X. Song, D. Ma, G. Yu, and X. Bao, Phys. Rev. C **113**, 014307 (2026)
[29] J. Patterson and R. Peterson, Nucl. Phys. A **717**, 235 (2003)
[30] J. Zhang, X. Tu, Y. Huang, *et al*., Comput. Phys. Commun. **312**, 109587 (2025)
[31] M. Park, Y. Choi, and Y. Kim, Int. J. Mod. Phys. E **34**, 2550021 (2025)
[32] Z. Yuan, D. Bai, Z. Wang, *et al*., Sci. Chin. Phys., Mech. Astron. **66**, 222012 (2023)
[33] J. M. Dong, H. F. Zhang, and G. Royer, Phys. Rev. C **79**, 054330 (2009)
[34] Y. Lim, X. Xia, and Y. Kim, Phys. Rev. C **93**, 014314 (2016)
[35] Q. Zhao, J. M. Dong, J. L. Song, *et al*., Phys. Rev. C **90**, 054326 (2014)
[36] J. L. Chen, J. Y. Xu, J. G. Deng, *et al*., Eur. Phys. J. A **55**, 214 (2019)
[37] Z. X. Zhang and J. M. Dong, Chin. Phys. C **42**, 014104 (2018)
[38] V. Dehghani and S. Alavi, Chin. Phys. C **42**, 104101 (2018)
[39] J. Dong, W. Zuo, J. Gu, *et al*., Phys. Rev. C **81**, 064309 (2010)
[40] M. R. Pahlavani and F. Ahmadvand, Int. J. Mod. Phys. E **32**, 2350036 (2023)
[41] G. G. Adamian, N. V. Antonenko, R. V. Jolos, *et al*., Int. J. Mod. Phys. E **5**, 191 (1996)
[42] W. Yahya and B. Falaye, Nucl. Phys. A **1015**, 122311 (2021)
[43] F. G. Kondev, M. Wang, W. J. Huang, *et al*., Chin. Phys. C **45**, 030001 (2021)
[44] M. Wang, W. J. Huang, F. G. Kondev, *et al*., Chin. Phys. C **45**, 030003 (2021)
[45] A. Adel and A. R. Abdulghany, Physica Scripta **96**, 125314 (2021)
[46] M. Pahlavani and S. Rahimi Shamami, Chinese Journal of Physics **66**, 733 (2020)
[47] Y.-Y. Xu, X.-Y. Hu, D.-X. Zhu, X.-J. Wu, P.-C. Chu, and X.-H. Li, Nuclear Science and Techniques **34**, 30 (2023)
[48] D. S. Delion and A. Dumitrescu, Phys. Rev. C **103**, 054325 (2021)
[49] D. S. Delion, Phys. Rev. C **80**, 024310 (2009)
[50] M. Ismail, A. Adel, A. Y. Ellithi, and M. A. Abbas, Chinese Physics C **50**, 1 (2026)
[51] D. N. Poenaru, R. A. Gherghescu, and W. Greiner, Phys. Rev. C **83**, 014601 (2011)